minerals

MDPI

Article

The Roof Safety under Large Mining Height Working Face: A Numerical and Theoretical Study

Xiaofang Wo [1,2], Guichen Li [1,2,*], Jinghua Li [1,2], Sen Yang [1,2], Zhongcheng Lu [1,2], Haoran Hao [1,2] and Yuantian Sun [1,2,3,*]

1 School of Mines, China University of Mining and Technology, Xuzhou 221116, China
2 Key Laboratory of Deep Coal Resource Mining of the Ministry of Education, China University of Mining and Technology, Xuzhou 221116, China
3 State Key Laboratory of Green and Low-Carbon Development of Tar-Rich Coal in Western China, Xi'an University of Science and Technology, Xi'an 710054, China
* Correspondence: liguichen@126.com (G.L.); yuantiansun@cumt.edu.cn (Y.S.)

Abstract: As an important technology of thick coal seam mining, fully mechanized mining with a large mining height has high mining efficiency. In order to study the roof safety control of large mining height working face, the 122,106 working face of Caojiatan coal mine is taken as the engineering background. The numerical simulation method is used to analyze the control ability of roof subsidence when the support strength is 1.2 MPa, 1.4 MPa, 1.6 MPa, 1.8 MPa, 2.0 MPa, and 2.2 MPa. The results show that the support strength of hydraulic support is negatively correlated with roof subsidence. Through theoretical analysis of the mechanical model of the support and surrounding rock under the filling condition, it is shown that the height of the gap between the filling body and roof is the main influencing factor of roof subsidence: the smaller the height of the gap between the filling body and roof, the better the control effect on the roof. Through numerical simulation, the roof subsidence and surface subsidence under different filling rates are analyzed. The results show that when the filling rate increases to 80% the control of roof subsidence achieves better results. Taking production safety and economic benefits into consideration, when the reasonable support strength of the working face is determined to be 2.0 MPa and the filling rate is 80%, the safety control of the working face roof can be ensured.

Keywords: large mining height; safety control; support strength; filling mining; roof subsidence

Citation: Wo, X.; Li, G.; Li, J.; Yang, S.; Lu, Z.; Hao, H.; Sun, Y. The Roof Safety under Large Mining Height Working Face: A Numerical and Theoretical Study. *Minerals* **2022**, *12*, 1217. https://doi.org/10.3390/min12101217

Academic Editor: Yosoon Choi

Received: 14 August 2022
Accepted: 13 September 2022
Published: 27 September 2022

1. Introduction

There are abundant thick coal seam resources in Western China. At present, the commonly used methods for thick coal seam mining in China mainly include layered mining, top coal caving mining, and large mining height technology [1–4]. Layered mining has the problem of high requirements for roadway layout, and roadway support is relatively difficult [5–7]. Top coal caving technology has the advantage of high mining efficiency for thick coal seams, but there are also problems such as low coal recovery rate, waste of resources, and increase of gangue content caused by inaccurate timing of top coal caving [8–11]. The state has increasingly strict control over resources and environmental protection, and pays increasing attention to the safety of the working face. The large mining height mining method has high efficiency and can mine the whole coal seam, which plays a large role in the emergence of ten-million-ton coal mines [12–14]. In terms of controlling surface subsidence and ensuring the safety of the working face, the hydraulic support with high working resistance is combined with the filling method; this is in line with national policy and future development trends.

At present, many scholars have conducted much research on the interaction between large mining height hydraulic support and surrounding rock [15–18]. Through the method of numerical simulation, scholars concluded that there is an exponential relationship between the maximum subsidence of the roof within the roof control range and the support strength of support [19,20]. Some scholars used the sensor monitoring method to study the relationship between the working resistance of the support and the roof subsidence [21,22]. It has been concluded that the high working resistance of the support can control the roof subsidence of the working face, but the roof support effect is not necessarily obvious after blindly increasing the working resistance.

Filling mining technology is mainly the technology of using corresponding filling materials to effectively control the rock stratum [23–25]. Although the cost of filling mining is high, it plays a large role in controlling rock movement, preventing surface collapse, liberating "three unders" pressed coal, and treating solid waste [26–29]. Many scholars believe that when studying the control of filling technology on surface subsidence, the coupling relationship between hydraulic support, roof, and filling body should be comprehensively considered. Some scholars established the mechanical relationship model and differential equation between support and surrounding rock under filling conditions according to the elastic foundation beam theory [30]. Other scholars have studied the control ability of roadway roof by using materials with different filling heights and filling strengths. The appropriate water–cement ratio and filling rate are determined through calculation and analysis [31–33]. Some scholars have studied the surface subsidence law and parameter prediction of fully mechanized mining face through the combination of theoretical analysis, engineering measurement, and numerical simulation. It can be concluded that filling rate is an important factor in determining filling quality [34].

The objective of this work is to use numerical calculation and numerical simulation methods to study the influence of support strength and filling rate on roof control when at 10 m mining height. As an important technology of future coal mining, the large mining height mining method needs more research regarding the roof control of super-high coal seams [35]. In Section 2, this paper takes the geological conditions of Caojiatan coal mine as an example to introduce the engineering background of the project. Then, in Section 3, a numerical model is established according to the physical and mechanical parameters of coal and rock strata. Section 4 studies the control ability of different support strengths on the roof in order to obtain the appropriate support strength. In Section 5, the control ability of different filling rates on roof subsidence and surface subsidence is analyzed to obtain the appropriate filling rate. The research results have certain reference significance for the determination of support strength and filling rate of large mining height working face under similar engineering conditions.

2. Project Overview

Caojiatan mine is located in the northeast of Ordos Plateau and the north of Loess Plateau, Northern Shaanxi. This paper takes the 122,106 working face of Caojiatan coal mine as the research object. The ground elevation of the 122,106 working face is +1285~+1329 m, the elevation of the mining face is +965~+990 m, the buried depth of the coal seam is 255~338 m, and the thickness of the coal seam is 9.93~12.09 m, with an average thickness of 11.01 m. The dip angle of the coal seam is 0°~5°, and the direct roof is dominated by fine-grained sandstone with an average thickness of 2 m. The main roof is dominated by siltstone with an average thickness of 7.31 m. The direct bottom is dominated by siltstone with an average thickness of 7.53 m, and the main bottom is dominated by fine–medium sandstone with an average thickness of 18.27 m. Figure 1 is the engineering background map of the working face.

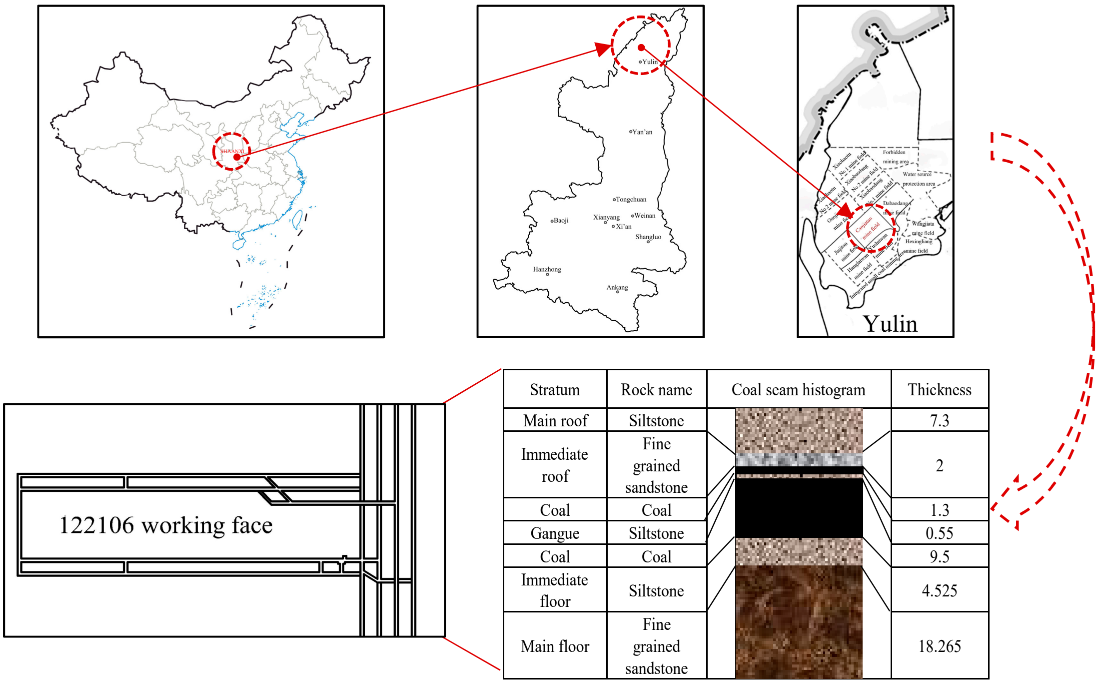

Figure 1. Project background.

3. Model Establishment

To study the control ability of hydraulic supports with different support strengths on the roof of goaf under the condition of large mining height, a model with a length of 400 m and height of 120 m is established using UDEC numerical simulation software, and the height of the coal seam is set as 10 m. According to existing parameters, the model is simplified to 10 layers. The buried depth of the model coal seam is 330 m. The coal seam is excavated 200 m, the mining height is 10 m, and 50 m boundaries are set on the left and right sides of the model. Taking the lower left corner of the model as the origin, a measuring point is positioned at the roof of the working face at x = 105 and y = 37, and a measuring point is positioned every 10 m within the upper boundary of the model from x = 80~320 m and y = 120 m. The vertical displacement of these measuring points is monitored to reflect the roof subsidence and surface subsidence. The support command is used to simulate the hydraulic support unit, and it is set in the goaf of the working face to simulate different support strengths. The model of hydraulic support is set as ZY37000/55/100, the support resistance of hydraulic support is about 37,000 kN, and the support strength is about 2 MPa. Figure 2 is the mechanical model of the numerical calculation. Physical and mechanical parameters of coal and rock stratum are shown in Table 1.

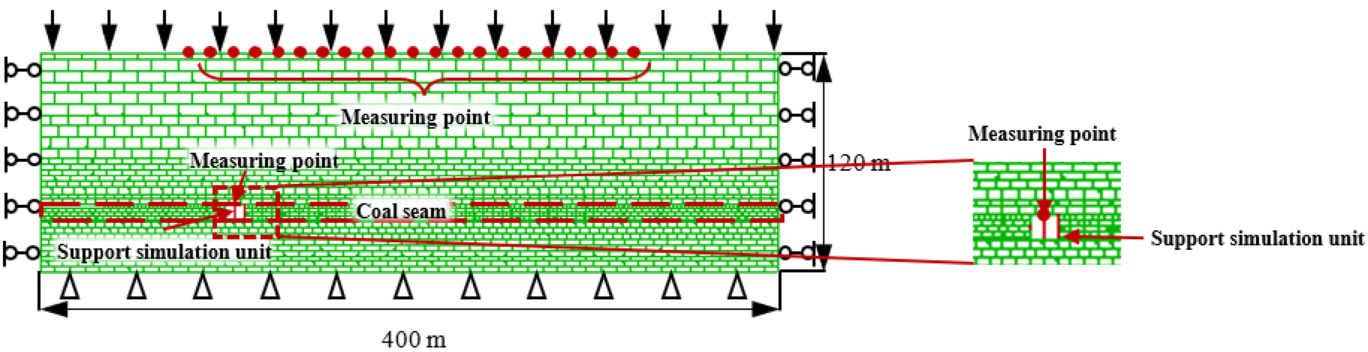

Figure 2. Mechanical model of numerical calculation.

Table 1. Physical and mechanical parameters of coal and rock strata.

Number	Rock Lithology	Thickness/m	Density/kg·m^{-3}	Bulk Modu-lus/GPa	Shear Mod-ulus/GPa	Friction Angle/°	Cohesion/MPa	Tensile Strength/MPa
1	Loess	34	1960	0.25	0.09	25	5.5	0.35
2	Medium-grained sandstone	24	2987	23.4	13	40	3.6	4.07
3	Fine-grained sandstone	12	2610	2.23	1.67	38	3	3.15
4	Siltstone	8	2558	6.32	3.61	33	4.7	3.07
5	Fine-grained sandstone	2	2610	2.23	1.67	38	3	3.15
6	Siltstone	3	2603	7	4	43	4.3	6.99
7	Filling body	2~8	1900	5.5	2.1	36	0.4	0.5
8	Coal	10	1445	7.1	4.9	22	1.44	2.4
9	Siltstone	9	2558	6.32	3.61	33	4.7	3.07
10	Fine-grained sandstone	18	2690	2.23	16.7	32	2.8	3.17

4. Study on Control of Roof Subsidence by Different Support Strengths

To study the control ability of different support strengths on roof and surface subsidence, we establish a UDEC model and insert a hydraulic support unit. Its influence on the roof subsidence and surface subsidence is then analyzed in order to determine the appropriate support strength. The roof subsidence and surface subsidence are simulated when the support strength is 1.2 MPa, 1.4 MPa, 1.6 MPa, 1.8 MPa, 2.0 MPa, and 2.2 MPa. Figure 3 shows the relationship between support strength and roof subsidence. Table 2 shows the roof subsidence parameters under different support strength conditions.

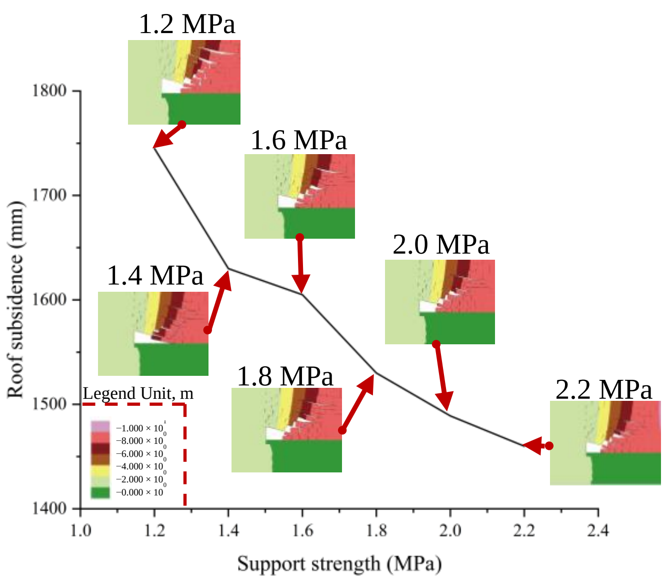

Figure 3. Relationship between support strength and roof subsidence.

Table 2. Roof subsidence parameters under different support strength conditions.

Support strength/MPa	1.2	1.4	1.6	1.8	2.0	2.2
Roof subsidence/mm	1745	1630	1605	1530	1489	1460

Figure 3 shows that there is a negative correlation between the support strength of hydraulic support and roof subsidence, that the overall shape of the change curve is downward convex, and that the curve is close to an exponential relationship. When the support strength is increased from 1.2 MPa to 1.8 MPa, the maximum subsidence of the roof within the roof control range is reduced from 1745 mm to 1530 mm (a reduction of 215 mm). When the support strength is increased from 1.8 MPa to 2.2 MPa, the maximum roof subsidence in the roof control area is reduced by a relatively small amount, from

1530 mm to 1460 mm (reduction of 70 mm). Therefore, the support strength has an obvious control effect on the roof subsidence in the roof control area, but there is a certain limit. When the support strength exceeds 1.8 MPa, the maximum roof subsidence of the working face tends to be stable. Considering production safety and economic benefits, the support strength is initially set at 2.0 MPa.

5. Study on the Control of Roof Subsidence and Surface Subsidence of Working Face under Different Filling Rates

According to the above analysis, when the support strength reaches 2.0 MPa the roof subsidence of the working face is 1489 mm, which still produces large deformation, with even greater roof deformation at the goaf. When combined with the filling mining method, the overburden is supported by coal, support, and filling. The support strength of the hydraulic support does not have a great impact on the breaking of the overlying strata in the whole goaf, but it plays a very important role in the roof subsidence control of the hydraulic support roof control area. The control ability of hydraulic support has certain limits. The control of the whole overburden is mainly determined by goaf filling. In the process of filling mining, the roof will deform with the mining and filling process, and will undergo bending and subsidence, as well as support of filling body and stability. In this process, the elastic foundation coefficient of the hydraulic support, the height of the gap between the filling body and roof, and the elastic foundation coefficient of the filling body will all affect the movement of the overlying rock. The model of common support of filling body, coal body, and hydraulic support, as well as the deflection differential equation of roof rock beam, are constructed based on the elastic foundation beam theory. The influence of various factors on the roof control ability is further analyzed according to the derivation of the formula. The following section is a detailed analysis of the mechanical model.

5.1. Mechanical Model of Support and Surrounding Rock under Filling Conditions

In this model, the upper part is under the stress of the equivalent uniformly distributed load q. The model is also supported by the supporting force $k_m y$ of the coal wall area on both sides, the supporting force $k_z y$ of the roof control area of the working face, and the supporting force $k_c y$ of the gob filling area. k_m is the elastic foundation coefficient of coal mass on both sides, k_z is the elastic foundation coefficient of the top control area of the hydraulic support, and k_c is the elastic foundation coefficient of the filling area. The main factors affecting the movement of overlying strata are the elastic foundation coefficient of the goaf roof area and the elastic foundation coefficient of the goaf filling body. Referring to the relevant literature, the differential equation of deflection of overburden rock beam of filling working face is as follows:

$$\begin{cases} EI\frac{d^4y}{dx^4} + k_m y = q & x \in (-L_1 - L_2, -L_2) \\ EI\frac{d^4y}{dx^4} + k_z y = q & x \in (-L_2, 0) \\ EI\frac{d^4(y-f_c)}{dx^4} + k_c(y - f_c) = q & x \in (0, L_3) \\ EI\frac{d^4y}{dx^4} + k_m y = q & x \in (L_3, L_3 + L_4) \end{cases} \tag{1}$$

where: E—Elastic modulus, GPa;

I—Moment of inertia, m^4;

k_m—Elastic foundation coefficient of coal, GN/m^3;

k_z—Elastic foundation coefficient of roof control area, GN/m^3;

k_c—Elastic foundation coefficient of backfill, GN/m^3;

f_c—The roof subsidence value in the case of filling mainly depends on the height of the gap between the filling body and roof, m;

L_1—Length of the coal wall area in front of working face, m;

L_2—Length of roof control area of working face, m;

L_3—Length of filling area, m;

L_4—Length of coal wall area behind the filling body, m.

According to Equation (1), with an increase of the thickness of the filling body f_c will decrease, hence the deflection of the top control area of the support will decrease (it will play a certain role in supporting the roof control area of the support, so as to control the roof subsidence of the working face).

Taking the characteristic coefficients as $\alpha = \sqrt[4]{k_m/4EI}$, $\beta = \sqrt[4]{k_z/4EI}$, and $\gamma = \sqrt[4]{k_c/4EI}$ and incorporating them into Equation (1), the general solution of the fourth-order non-homogeneous differential equation is:

$$y = \begin{cases} e^{\alpha x}[A_1\sin(\alpha x) + A_2\cos(\alpha x)] + e^{-\alpha x}[A_3\sin(\alpha x) + A_4\cos(\alpha x)] + \frac{q}{k_m} & x \in (-L_1 - L_2, -L_2) \\ e^{\beta x}[B_1\sin(\beta x) + B_2\cos(\beta x)] + e^{-\beta x}[B_3\sin(\beta x) + B_4\cos(\beta x)] + \frac{q}{k_z} & x \in (-L_2, 0) \\ e^{-\gamma x}[C_1\sin(\gamma x) + C_2\cos(\gamma x)] + e^{\gamma x}[C_3\sin(\gamma x) + C_4\cos(\gamma x)] + \frac{q}{k_c} + f_c & x \in (0, L_3) \\ e^{-\alpha x}[D_1\sin(\alpha x) + D_2\cos(\alpha x)] + e^{\alpha x}[D_3\sin(\alpha x) + D_4\cos(\alpha x)] + \frac{q}{k_m} & x \in (L_3, L_3 + L_4) \end{cases} \quad (2)$$

When $x \le 0$, if $x \to -\infty$ satisfies that y is a finite value, there is $A_3 = A_4 = B_3 = B_4 = 0$; when $x \ge 0$, if $x \to +\infty$ satisfies that y is a finite value, then there is $C_3 = C_4 = D_3 = D_4 = 0$. The deflection equation can be simplified as:

$$y = \begin{cases} e^{\alpha x}[A_1\sin(\alpha x) + A_2\cos(\alpha x)] + \frac{q}{k_m} & x \in (-L_1 - L_2, -L_2) \\ e^{\beta x}[B_1\sin(\beta x) + B_2\cos(\beta x)] + \frac{q}{k_z} & x \in (-L_2, 0) \\ e^{-\gamma x}[C_1\sin(\gamma x) + C_2\cos(\gamma x)] + \frac{q}{k_c} + f_c & x \in (0, L_3) \\ e^{-\alpha x}[D_1\sin(\alpha x) + D_2\cos(\alpha x)] + \frac{q}{k_m} & x \in (L_3, L_3 + L_4) \end{cases} \quad (3)$$

The relationship between the rotation angle $\theta(x)$, bending moment $M(x)$, shear force $Q(x)$, and deflection y of the top beam section is as follows:

$$\begin{cases} \theta(x) = \frac{dy}{dx} \\ M(x) = -EI\frac{d^2y}{dx^2} \\ Q(x) = -EI\frac{d^3y}{dx^3} \end{cases} \quad (4)$$

According to the continuity conditions at the junction $x = -L_2$, $x = 0$, and $x = L_3$:

$$\begin{cases} y_1(-L_2) = y_2(-L_2) \\ \theta_1(-L_2) = \theta_2(-L_2) \\ M_1(-L_2) = M_2(-L_2) \\ Q_1(-L_2) = Q_2(-L_2) \end{cases} \begin{cases} y_2(0) = y_3(0) \\ \theta_2(0) = \theta_3(0) \\ M_2(0) = M_3(0) \\ Q_2(0) = Q_3(0) \end{cases} \begin{cases} y_3(L_3) = y_4(L_3) \\ \theta_3(L_3) = \theta_4(L_3) \\ M_3(L_3) = M_4(L_3) \\ Q_3(L_3) = Q_4(L_3) \end{cases} \quad (5)$$

Next we bring the equations into the numerical calculation software Maple, take the values of the unknown parameters in Equation (1) (as shown in Table 3), and bring the relevant parameters into Equations (3)–(5); through this process, specific parameters A_1, A_2, B_1, B_2, C_1, C_2, D_1, and D_2 of each paragraph can be obtained. The parameters are brought into Equation (3) to solve the deflection curve equation of the roof rock beam of the filling working face. Figure 4 shows the influence curve of different factors on roof subsidence.

Table 3. Value range of influencing factors of roof subsidence.

Average Volume Force of Overburden γ/(kN/m^3)	Elastic Foundation Coefficient of Coal k_m/(GN/m^3)	Elastic Foundation Coefficient of Hydraulic Support k_z/(GN/m^3)	Elastic Foundation Coefficient of Backfill k_c/(GN/m^3)	Elastic Modulus of Direct Roof Rock Beam E/GPa	Height of Gap between Filling Body and Roof f_c/m
25	0.2~0.6	0.28~0.52	0.05~0.3	5~20	2~10

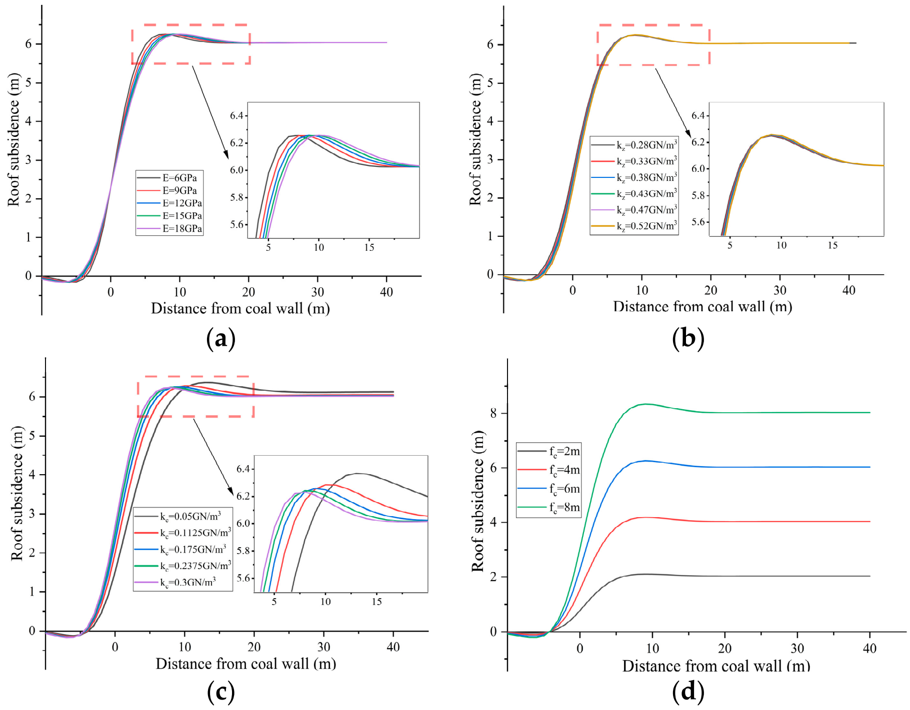

Figure 4. (**a**) Influence of elastic modulus of the direct roof on roof subsidence. (**b**) Influence of elastic foundation coefficient of support on roof subsidence. (**c**) Influence of elastic foundation coefficient of filling body on roof subsidence. (**d**) Influence of height of the gap between filling body and roof on roof subsidence.

It can be seen from Figure 4a that the elastic modulus of the direct roof has little effect on the roof subsidence. As the elastic modulus decreases, the roof subsidence reaches its peak value and reaches the stable state more quickly. The elastic modulus of the direct roof ranges from 6 GPa to 18 GPa. When the elastic modulus is 6 GPa and 18 GPa, the position where the peak value occurs is 7.5 and 10 m away, respectively. When the height of the gap between the filling body and roof is 6 m, the final stable value of roof subsidence tends to be 6.03 m, indicating that the elastic modulus of the direct roof has little effect on roof subsidence.

Figure 4b shows that the elastic foundation coefficient of the support has little influence on the roof subsidence. When the elastic foundation coefficient of the support changes within the range of 0.28~0.52 GN/m^3 it has little influence on the roof subsidence.

As can be seen from Figure 4c, where k_c is in the range of 0.05~0.3 GN/m^3, when the height of the gap between the filling body and roof is 6 m the variation range of the peak value of roof subsidence is 6.2~6.4 m. When it is close to the working face, the greater the value of k_c, the greater the roof subsidence and the greater the roof subsidence rate. After exceeding a certain range, the greater the value of k_c, the smaller the roof subsidence. Analysis provides the reason: when it is close to the working face, the roof displacement is jointly controlled by the support and filling body, while when it is far from the working face the roof displacement is only affected by the filling body.

It can be seen from Figure 4d that the height of the gap between the filling body and roof f_c has a great impact on the final subsidence of the roof. When f_c is 2 m, 4 m, 6 m, and 8 m, the maximum subsidence of the gob roof is 2.1 m, 4.2 m, 6.25 m, and 8.3 m, respectively. It is apparent that the larger the filling height, the smaller the maximum subsidence value of the corresponding roof. When f_c is controlled within a certain range, it will not cause large subsidence of the roof.

5.2. Study on Control of Roof Subsidence and Surface Subsidence of Working Face under Different Filling Rates

When the support strength of the hydraulic support is 2.0 MPa, the roof deformation of the working face is 1489 mm, and the roof deformation is still large. To effectively control the roof of the working face and goaf, the influence of the filling rate of goaf on the control of roof subsidence and surface subsidence of the working face is studied below. Figure 5 shows the displacement nephogram, stress nephogram, and plastic zone nephogram of the overall model under filling rates of 20%, 40%, 60%, and 80%.

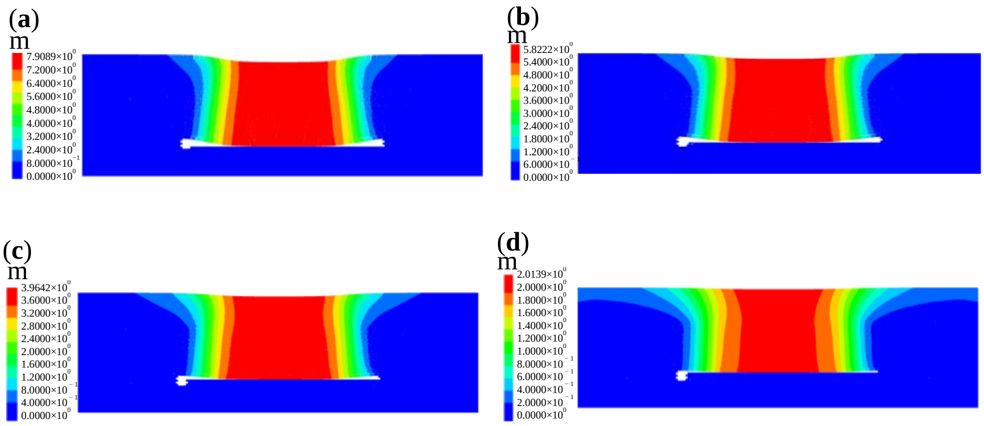

Figure 5. (**a**) Displacement nephogram with the filling rate of 20%. (**b**) Displacement nephogram with filling rate of 40%. (**c**) Displacement nephogram with the filling rate of 60%. (**d**) Displacement nephogram with a filling rate of 80%.

Figure 6 presents displacement nephograms under different filling rates under the condition of large mining height. Figure 6 shows that when the filling rate is 20%, the roof subsidence of the working face is 1250 mm; when the filling rate is 40%; the roof subsidence of the working face is 937 mm; when the filling rate is 60%, the roof subsidence of the working face is 687 mm; and when the filling rate is 80%, the roof subsidence of the working face is 387 mm. Therefore, good control of the working face roof is achieved at a filling rate of 60%, and the best control is achieved at a filling rate of 80%.

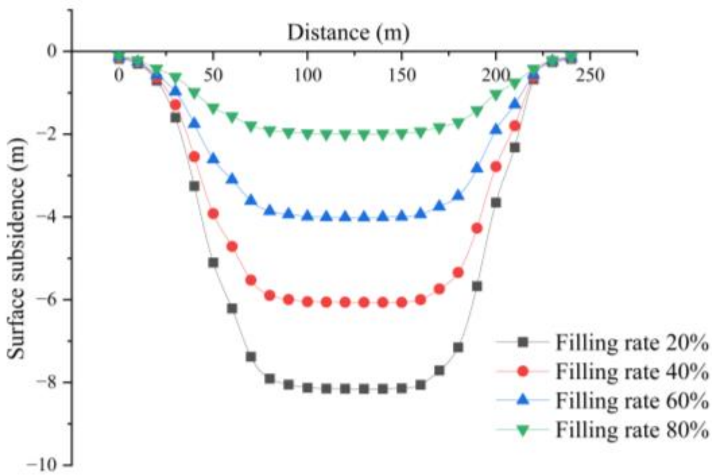

Figure 6. Upper boundary subsidence curves of the model at different filling rates.

Figure 7 shows stress nephograms under the conditions of different filling rates. It can be seen from the figure that there are stress concentration areas in the coal wall in front of the working face and behind the open cut hole, and the stress in the middle of the overall goaf also shows obvious stress concentration due to the stress of the overlying strata. When the filling rate is 20%, the influence of the mining stress of overlying strata in goaf is large, and the roof subsidence of goaf is large. As the filling rate gradually increases from 40% to 60% and 80%, the filling body bears the load of the overlying strata more effectively, and the influence range of the stress change of the overlying strata also decreases.

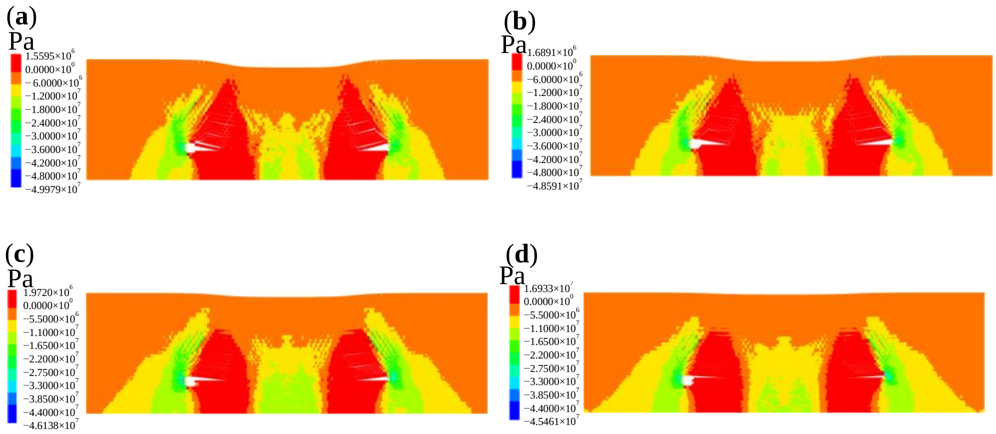

Figure 7. (**a**) Stress nephogram with a filling rate of 20%. (**b**) Stress nephogram with a filling rate of 40%. (**c**) Stress nephogram with a filling rate of 60%. (**d**) Stress nephogram with a filling rate of 80%.

It can be seen from Figure 8 that when the filling rate is 20%, 40%, 60%, and 80%, the tensile failure degree of the overlying rock layer gradually decreases. The development height of fracture zone also gradually decreases, the bending subsidence zone above the fracture zone decreases with the increase of the filling rate of the goaf, and the deformation of the bending subsidence zone above the fracture zone also gradually decreases. When the filling rate is 20% and 40%, an obvious three-zone structure can be seen. When the filling rate reaches 60% and 80%, the filling body occupies the collapsed space of the original overburden, so a certain degree of rock stratum control is achieved. The filling effect is better when the filling rate is 80%.

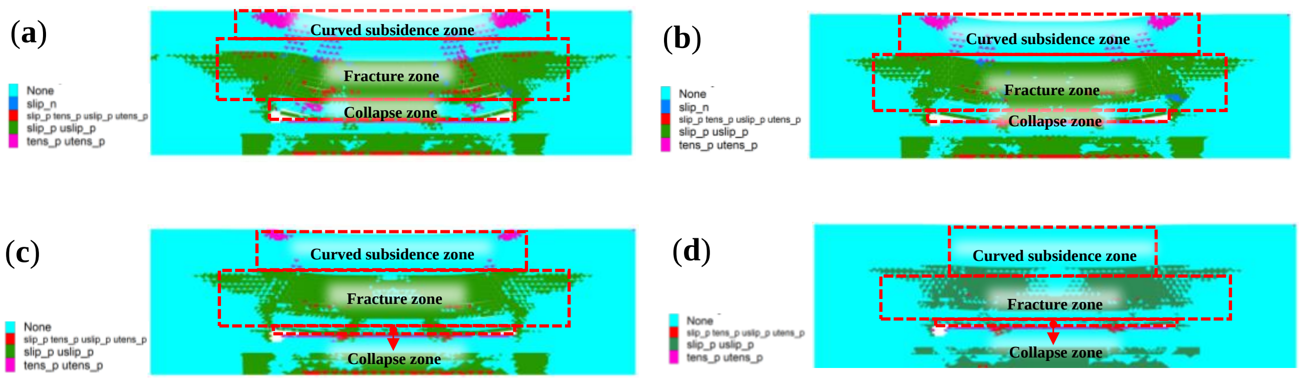

Figure 8. (**a**) Plastic zone diagram with a filling rate of 20%. (**b**) Plastic zone diagram with a filling rate of 40%. (**c**) Plastic zone diagram with a filling rate of 60%. (**d**) Plastic zone diagram with a filling rate of 80%.

6. Conclusions

(1) With the increase of support strength, the maximum roof subsidence of the working face gradually decreases. When the support strength is 2.0 MPa, the roof subsidence of the working face is 1489 mm. When the support strength increases to 2.2 MPa, the roof subsidence is 1460 mm, and the reduction range of roof subsidence is very small. Therefore, we select the support strength of 2.0 MPa.

(2) By establishing the mechanical model of support and surrounding rock, the effects of direct roof elastic modulus E, support elastic foundation coefficient k_z, filling elastic

foundation coefficient k_c, and height of the gap between filling body and roof f_c on roof subsidence are analyzed. The changes of E and k_z have little effect on the roof subsidence. When it is close to the working face, the greater the value of k_c, the greater the roof subsidence. When it is far from the working face, the roof subsidence is almost only affected by the filling rate. When f_c is 2 m, 4 m, 6 m, and 8 m, the maximum subsidence of the gob roof is 2.1 m, 4.2 m, 6.25 m, and 8.3 m, respectively. This indicates that with an increase of the thickness of the filling body, the deflection of the support control area will decrease, which achieves the purpose of roof safety control.

(3) When filling the goaf, the method adopted is immediate filling after model excavation. Through the analysis of displacement nephogram, stress nephogram and plastic zone diagram under different filling rates, and the monitoring of roof subsidence, determine the appropriate filling rate. Measuring points are positioned on the roof of the working face and upper boundary of the model to monitor the roof subsidence and surface subsidence of the model. By analyzing the surface subsidence curves under the conditions of different filling rates, it is found that the surface control effect is best when the filling rate is 80%.

Author Contributions: Conceptualization, X.W., G.L. and Y.S.; methodology, X.W., G.L. and Y.S.; formal analysis, J.L., S.Y., Z.L. and H.H.; investigation, J.L., S.Y., Z.L. and H.H.; writing—original draft preparation, X.W.; supervision, G.L. and Y.S.; funding acquisition, G.L. All authors have read and agreed to the published version of the manuscript.

Funding: This research was funded by the projects of The Fundamental Research Funds for the Central Universities (2020ZDPY0221, 2021QN1003); National Natural Science Foundation of China (52104106, 52174089); Basic Research Program of Xuzhou (KC21017); and State Key Laboratory of Green and Low-carbon Development of Tar-rich Coal in Western China, Xi'an University of Science and Technology, SKLCRKF21-08.

Conflicts of Interest: The authors declare that they have no competing interest.

References

1. Kong, D.Z.; Cheng, Z.B.; Zheng, S.S. Study on the failure mechanism and stability control measures in a large-cutting-height coal mining face with a deep-buried seam. *Bull. Eng. Geol. Environ.* **2019**, *78*, 6143–6157. [CrossRef]
2. Le, T.D.; Zhang, C.G.; Oh, J.; Mitra, R.; Hebblewhite, B. A new cavability assessment for Longwall Top Coal Caving from discontinuum numerical analysis. *Int. J. Rock Mech. Min. Sci.* **2019**, *115*, 11–20. [CrossRef]
3. Huang, P.; Ju, F.; Jessu, K.V.; Xiao, M.; Guo, S. Optimization and Practice of Support Working Resistance in Fully-Mechanized Top Coal Caving in Shallow Thick Seam. *Energies* **2017**, *10*, 1406. [CrossRef]
4. Zhang, Q.Y.; Du, T. Research on and Application of Roof Management Technology in 8.8m Ultra-high Fully Mechanized Mining Face. In Proceedings of the Iop 5th International Conference on Materials Science, Energy Technology and Environmental Engineering (MSETEE), Electr Network, Shanghai, China, 7–9 August 2020; Iop Publishing Ltd.: Shanghai, China, 2020.
5. Li, Z.L.; He, X.Q.; Dou, L.M.; Song, D.Z. Comparison of rockburst occurrence during extraction of thick coal seams using top-coal caving versus slicing mining methods. *Can. Geotech. J.* **2018**, *55*, 1433–1450. [CrossRef]
6. Fu, J.H.; Wen, G.C.; Sun, H.T.; Yang, X.L. Study on the shear movement law of overlying strata by slice mining. *Energy Sci. Eng.* **2020**, *8*, 2335–2351. [CrossRef]
7. Baryshnikov, V.D.; Gakhova, L.N. Stress-strain state of adjacent rock mass under slice mining of steeply dipping ore bodies. In Proceedings of the Conference on Geodynamics and Stress State of the Earth's Interior (GSSEI), Russian Acad Sci, Siberian Branch, Inst Mining, Novosibirsk, Russia, 2–4 October 2017; Iop Publishing Ltd.: Novosibirsk, Russia, 2017.
8. Li, Z.L.; He, X.Q.; Dou, L.M.; Song, D.Z.; Wang, G.F. Numerical investigation of load shedding and rockburst reduction effects of top-coal caving mining in thick coal seams. *Int. J. Rock Mech. Min. Sci.* **2018**, *110*, 266–278. [CrossRef]
9. Song, Z.Y.; Konietzky, H.; Herbst, M. Drawing mechanism of fractured top coal in longwall top coal caving. *Int. J. Rock Mech. Min. Sci.* **2020**, *130*, 13. [CrossRef]
10. Zhang, B.S.; Yang, Z.P.; Ji, C.X.; Guo, Z.F.; Li, H.Y. Research on the Influence of the Key Stratum Position on the Support Working Resistance during Large Mining Height Top-Coal Caving Mining. *Adv. Civ. Eng.* **2021**, *2021*, 6690280. [CrossRef]
11. Yang, L.; Li, L.H.; Wei, W.J. Optimization of Caving Technology in an Extrathick Seam with Longwall Top Coal Caving Mining. *Adv. Mater. Sci. Eng.* **2021**, *2021*, 7725159. [CrossRef]
12. Wen, Z.J.; Xing, E.R.; Shi, S.S.; Jiang, Y.J. Overlying strata structural modeling and support applicability analysis for large mining-height stopes. *J. Loss Prev. Process Ind.* **2019**, *57*, 94–100. [CrossRef]

13. Yuan, H.H.; Shan, R.L.; Su, X.G. Deformation characteristics and stability control of a gateroad in fully mechanized mining with large mining height. *Arab. J. Geosci.* **2018**, *11*, 15. [CrossRef]
14. Wu, F.F.; Yue, X.; Yang, J.X.; Du, B.J.; Zhang, J.; Lv, B. Model of Overlying Strata Structure in Large Mining Height Excavating Condition and Calculation of Support Working Resistance. *Geofluids* **2022**, *2022*, 5894735. [CrossRef]
15. Cheng, F.; Chen, A.J.; Wu, D.; Tang, X.Y.; Su, C.H. Numerical Simulation of Cracking Failure and Weakening Law of Roadway Surrounding Rock under High Stress. *Shock Vib.* **2021**, *2021*, 7236077. [CrossRef]
16. Gao, M.S.; He, Y.L.; Xu, D.; Yu, X. A New Theoretical Model of Rock Burst-Prone Roadway Support and Its Application. *Geofluids* **2021**, *2021*, 5549875. [CrossRef]
17. Zhang, K.; Li, Y.X.; Feng, L.; Meng, X.J.; Zhong, D.H.; Huang, L.S. Roof deformation characteristics and experimental verification of advanced coupling support system supporting roadway. *Energy Sci. Eng.* **2022**, *10*, 2397–2419. [CrossRef]
18. Sun, Y.T.; Li, G.C.; Zhang, J.F.; Yao, B.C.; Qian, D.Y.; Huang, J.D. Numerical Investigation on Time-Dependent Deformation in Roadway. *Adv. Civ. Eng.* **2021**, *2021*, 4280139. [CrossRef]
19. Li, G.; Ma, F.S.; Guo, J.; Zhao, H.J.; Liu, G. Study on deformation failure mechanism and support technology of deep soft rock roadway. *Eng. Geol.* **2020**, *264*, 15. [CrossRef]
20. Wang, Q.; Jiang, B.; Pan, R.; Li, S.C.; He, M.C.; Sun, H.B.; Qin, Q.; Yu, H.C.; Luan, Y.C. Failure mechanism of surrounding rock with high stress and confined concrete support system. *Int. J. Rock Mech. Min. Sci.* **2018**, *102*, 89–100. [CrossRef]
21. Liu, W.T.; Pang, L.F.; Xu, B.C.; Sun, X. Study on overburden failure characteristics in deep thick loose seam and thick coal seam mining. *Geomat. Nat. Hazards Risk* **2020**, *11*, 632–653. [CrossRef]
22. Wang, J.C.; Wang, Z.H. Systematic principles of surrounding rock control in longwall mining within thick coal seams. *Int. J. Min. Sci. Technol.* **2019**, *29*, 65–71. [CrossRef]
23. Chen, Y.; Li, D.; Jiang, F.X.; Zhang, L.L.; Wang, C.W.; Zhu, S.T. Use of the Equivalent Mining Height Method for Understanding Overlying Strata Movement and Stress Distribution in an Isolated Coal Pillar. *Shock Vib.* **2020**, *2020*, 8820886. [CrossRef]
24. Wang, H.W.; Wu, Y.P.; Liu, M.F.; Jiao, J.Q.; Luo, S.H. Roof-breaking mechanism and stress-evolution characteristics in partial backfill mining of steeply inclined seams. *Geomat. Nat. Hazards Risk* **2020**, *11*, 2006–2035. [CrossRef]
25. Lin, H.; Yang, R.S.; Lu, B.; Li, Y.L.; Fang, S.Z.; Fan, Z.Y.; Li, Z.Z. Overlying strata movement law of continuous mining and continuous backfilling cemented-fill mining. *Environ. Earth Sci.* **2021**, *80*, 15. [CrossRef]
26. Yu, H.X.; Li, S.; Wang, X.M. The Recent Progress China Has Made in the Backfill Mining Method, Part III: Practical Engineering Problems in Stope and Goaf Backfill. *Minerals* **2022**, *12*, 88. [CrossRef]
27. Chang, Q.L.; Sun, Y.F.; Leng, Q.; Liu, Z.X.; Zhou, H.Q.; Sun, Y.T. Stability Analysis of Paste Filling Roof by Cut and Fill Mining. *Sustainability* **2021**, *13*, 10899. [CrossRef]
28. Tan, L.H.; Zhou, Z.L.; Cai, X.; Rui, Y.C. Analysis of mechanical behaviour and fracture interaction of multi-hole rock mass with DIC measurement. *Measurement* **2022**, *191*, 18. [CrossRef]
29. Sang, P.D. Research and Application of Green Filling Mining Technology for Short Wall Mining in Aging Mine. In Proceedings of the Iop 4th International Workshop on Renewable Energy and Development (IWRED), Electr Network, Sanya, China, 24–26 April 2020; Iop Publishing Ltd.: Sanya, China, 2020.
30. Chen, D.D.; Wu, X.Y.; Xie, S.R.; Sun, Y.D.; Zhang, Q.; Wang, E.; Sun, Y.H.; Wang, L.; Li, H.; Jiang, Z.S.; et al. Study on the Thin Plate Model with Elastic Foundation Boundary of Overlying Strata for Backfill Mining. *Math. Probl. Eng.* **2020**, *2020*, 8906091. [CrossRef]
31. Zhu, X.J.; Guo, G.L.; Liu, H.; Yang, X.Y. Surface subsidence prediction method of backfill-strip mining in coal mining. *Bull. Eng. Geol. Environ.* **2019**, *78*, 6235–6248. [CrossRef]
32. Sun, Y.T.; Bi, R.Y.; Sun, J.B.; Zhang, J.F.; Taherdangkoo, R.; Huang, J.D.; Li, G.C. Stability of roadway along hard roof goaf by stress relief technique in deep mines: A theoretical, numerical and field study. *Geomech. Geophys. Geo-Energy Geo-Resour.* **2022**, *8*, 16. [CrossRef]
33. Cai, W.Y.; Chang, Z.C.; Zhang, D.S.; Wang, X.F.; Cao, W.H.; Zhou, Y.Z. Roof filling control technology and application to mine roadway damage in small pit goaf. *Int. J. Min. Sci. Technol.* **2019**, *29*, 477–482. [CrossRef]
34. Sun, Y.T.; Bi, R.Y.; Chang, Q.L.; Taherdangkoo, R.; Zhang, J.F.; Sun, J.B.; Huang, J.D.; Li, G.C. Stability Analysis of Roadway Groups under Multi-Mining Disturbances. *Appl. Sci.* **2021**, *11*, 7953. [CrossRef]
35. Li, G.C.; Sun, Y.T.; Qi, C.C. Machine learning-based constitutive models for cement-grouted coal specimens under shearing. *Int. J. Min. Sci. Technol.* **2021**, *31*, 813–823. [CrossRef]